INTERNATIONAL JOURNAL OF
NUMERICAL ANALYSIS AND MODELING
Volume 00, Number 0, Pages 000–000

A SIMPLE FAST ALGORITHM FOR MINIMIZATION OF THE ELASTICA ENERGY COMBING BINARY AND LEVEL SET REPRESENTATIONS

XUE-CHENG TAI AND JINMING DUAN

Abstract. For curves or general interfaces, Euler's elastica energy has a wide range of applications in computer vision and image processing. It is however difficult to minimize the functionals related to the elastica energy due to its non-convexity, nonlinearity and higher order with derivatives. In this paper, we propose a very simple way to combine level set and binray representations for interfaces and then use a fast algorithm to minimize the functionals involving the elastica energy. The proposed algorithm essentially just needs to solve a total variation type minimization problem and a re-distance problem. Nowadays, there are many fast algorithms to solve these two problems and thus the overall efficiency of the proposed algorithm is very high. We then apply the new Euler's elastica minimization algorithm to image segmentation, image inpainting and illusory shape reconstruction problems. Extensive experimental results are finally conducted to validate the effectiveness of the proposed algorithm.

Key Words. Euler's elastica energy, image segmentation, image inpainting, illusory shape, corner fusion, level set method, binary level set method, fast sweeping.

1. Introduction

For a two-dimensional curve γ, its elastica energy is defined as

$$E(\gamma) = \int_\gamma \left(a + b\kappa^2\right) ds. \tag{1}$$

Here κ is the curvature of the curve γ, ds is arc length and a and b are two positive parameters. If we set $b = 0$, $E(\gamma)$ measures the total length of the curve. If $a = 0$, then $E(\gamma)$ measures the twisting energy of the curve which is related to the curvature. The elastica energy has no difficulty to be extended for higher dimensional interface problems. For a function u defined on the domain Ω, the Euler's elastica energy of all level curves of u over Ω can be expressed as a functional of u by

$$E(u) = \int_\Omega \left(a + b\left|\nabla \cdot \frac{\nabla u}{|\nabla u|}\right|^2\right) |\nabla u| \, dx. \tag{2}$$

In the field of image processing, Euler's elastica energy was first introduced by Nitzberg, Mumford, and Shiota for segmenting an image into objects with different depths in the scene [1]. Since then, it has been adapted to many fundamental problems in mathematical imaging. This includes image inpainting [2, 3, 4], image restoration [5, 6, 4, 7], image zooming [4] and image segmentation [8, 9, 10].

It is however nontrivial to minimize the functional (2) directly, because it involves non-differentiable, nonlinear and higher order terms. Recently, a lot of research have focused on the developments of fast and reliable numerical methods for minimizing curvature based functionals, including the multigrid algorithm [11], the homotopy method [12], augmented Lagrangian method (ALM) based algorithms [13, 14, 4], graph cut based algorithms [7, 15] and convex relaxation approaches [16, 17, 18, 19]. Among them the ALM based algorithms are particularly of interest, because the resulting minimization problems by the ALM can be implemented very easily and efficiently. ALM thus has become a powerful tool for developing efficient numerical schemes to deal with many nonlinear image processing models, such as the non-differentiable Rudin-Osher-Fatemi (ROF) model [20], the Euler's elastica and mean curvature models [4, 9, 14, 21]. The main idea of the ALM is to convert the original problem into a few subproblems, each of which is a very simple problem and can thus be solved efficiently. The minimizer of the original problem is obtained when the overall algorithm has converged. To minimize the Euler's elastica energy (2) with a data fidelity term $\mathcal{D}(u)$ using the ALM, (2) is first transformed into the following equivalent constrained minimization problem

$$\min_{u,\boldsymbol{p},\boldsymbol{m},\boldsymbol{n}} \int_\Omega \left(a + b(\nabla\cdot\boldsymbol{n})^2\right)|\boldsymbol{p}|\,dx + \mathcal{D}(u) \;\; s.t.\; \boldsymbol{p} = \nabla u,\; \boldsymbol{n} = \tfrac{\boldsymbol{p}}{|\boldsymbol{p}|}. \tag{3}$$

The constraint $\boldsymbol{n} = \frac{\boldsymbol{p}}{|\boldsymbol{p}|}$ in (3) can be converted to

$$|\boldsymbol{m}| \le 1, \quad |\boldsymbol{p}| = \boldsymbol{m}\cdot\boldsymbol{p}, \quad \boldsymbol{m} = \boldsymbol{n}.$$

With these new constraints, the augmented Lagrangian functional for (3) is:

$$\begin{aligned} E\left(u,\boldsymbol{p},\boldsymbol{m},\boldsymbol{n};\lambda_1,\boldsymbol{\lambda_2},\boldsymbol{\lambda_3}\right) = &\int_\Omega \left(a + b(\nabla\cdot\boldsymbol{n})^2\right)|\boldsymbol{p}|\,dx + \mathcal{D}(u) \\ &+ \mu_1\int_\Omega (|\boldsymbol{p}| - \boldsymbol{p}\cdot\boldsymbol{m})dx + \int_\Omega \lambda_1\left(|\boldsymbol{p}| - \boldsymbol{p}\cdot\boldsymbol{m}\right)dx \\ &+ \frac{\mu_2}{2}\int_\Omega |\boldsymbol{p} - \nabla u|^2 dx + \int_\Omega \boldsymbol{\lambda_2}\cdot(\boldsymbol{p} - \nabla u)dx \\ &+ \frac{\mu_3}{2}\int_\Omega |\boldsymbol{n} - \boldsymbol{m}|^2 dx + \int_\Omega \boldsymbol{\lambda_3}\cdot(\boldsymbol{n} - \boldsymbol{m})dx + \delta_{\mathcal{R}}(\boldsymbol{m}) \end{aligned} \tag{4}$$

where $\mathcal{R} = \left\{m \in L^2(\Omega) : |m| \le 1 \text{ a.e. in } \Omega\right\}$ and $\delta_{\mathcal{R}}(\boldsymbol{m})$ is the characteristic function on the convex set $\mathcal{R}$, which is given by

$$\delta_{\mathcal{R}}(\boldsymbol{m}) = \begin{cases} 0 & \text{if } \boldsymbol{m} \in \mathcal{R} \\ +\infty & \text{otherwise} \end{cases}.$$

Moreover, μ_1, μ_2 and μ_3 are positive penalty parameters while λ_1, $\boldsymbol{\lambda_2}$ and $\boldsymbol{\lambda_3}$ are Lagrange multipliers. Since $\boldsymbol{m}$ is forced to be inside $\mathcal{R}$, $|\boldsymbol{m}| \le 1$, $|\boldsymbol{p}| - \boldsymbol{m}\cdot\boldsymbol{p} \ge 0$ for any $\boldsymbol{p}$, and $|\boldsymbol{p}| - \boldsymbol{m}\cdot\boldsymbol{p} = 0$ if and only if $\boldsymbol{m} = \frac{\boldsymbol{p}}{|\boldsymbol{p}|}$. This simplifies $\boldsymbol{p}$'s subproblem because quadratic term is avoided. The unknown $\boldsymbol{m}$ is introduced to decouple $\boldsymbol{p}$ and $\boldsymbol{n}$ such that $\boldsymbol{p}$'s subproblem can be solved by the shrinkage and $\boldsymbol{m}$'s subproblem by the fast Fourier transform. Notice that the fidelity term $\mathcal{D}(u)$ should be addressed properly according to different applications. For example, for noise removal with Gaussian noise, it is common to choose $\mathcal{D}(u) = \int_\Omega (u-f)^2 dx$. In such a case, the algorithm can be used directly and give fast numerical implementations. However, an additional variable should be introduced for the algorithm when $\mathcal{D}(u) = \int_\Omega |u-f|dx$, which is common for impulsive noise removal. We refer the reader to [4] for more details on the application of the ALM to different $\mathcal{D}(u)$. One now needs to minimize the augmented Lagrangian functional for each of the

variables $u, \boldsymbol{p}, \boldsymbol{m}, \boldsymbol{n}$ by fixing the others. After all the variables are solved, the Lagrange multipliers $\lambda_1, \boldsymbol{\lambda_2}, \boldsymbol{\lambda_3}$ should be updated. The procedure is repeated until all the variables have converged.

By considering the underlying relation between the length term and the curvature term in the Euler's elastica energy, in this paper we propose a novel algorithm for different image processing applications using the elastica energy. The proposed algorithm has several advantages:

- It has fewer parameters and therefore significantly reduces the effort of choosing appropriate parameters for obtaining desirable results.
- For image segmentation, it uses the relaxed binary representation for the length term and the signed distance representation for the calculation of curve curvature. Consequently, the original elastica problem boils down to a total variation type minimization problem and a re-distance problem, which can be solved efficiently with existing approaches.
- In addition to image segmentation, it can be easily extended to binary image inpainting and illusory shape problems.

In the following, we shall introduce the proposed algorithm in detail.

2. Euler's Elastica Energy Minimization for Segmentation, Inpainting and Illusory Shape Reconstruction

In this section, we shall explain the details in using the new algorithm to minimize the Euler's elastica energy for different imaging applications. We start with image segmentation, followed by image inpainting and illusory shape reconstruction.

2.1. Image Segmentation. For image segmentation, the authors in [9] suggested to substitute the regularisation term in the conventional Chan-Vese model with the Euler's elastica regulariser (2) and propose to solve

$$\min_{u\in[0,1]} \int_\Omega \left(\alpha + \beta\left|\nabla\cdot\frac{\nabla u}{|\nabla u|}\right|^2\right)|\nabla u|\,dx + \int_\Omega Q(c_1,c_2)u dx. \tag{5}$$

Note that $\mathcal{D}(u) = \int_\Omega Q(c_1,c_2)u dx$ in this case, where c_1 and c_2 are two constants which are known already and $Q(c_1,c_2) = (c_1-f)^2 - (c_2-f)^2$ for a given input image f. This fidelity term is the same as in the original Chan-Vese model [22]. In [9], (5) is optimised by the ALM introduced in the last section.

Alternatively, one can also use variational level set method to solve the same segmentation problem [23, 24]. The corresponding minimization model is:

$$\min_{\phi} \int_\Omega \left(\alpha + \beta\left|\nabla\cdot\frac{\nabla \phi}{|\nabla \phi|}\right|^2\right)|\nabla H(\phi)|\,dx + \int_\Omega Q(c_1,c_2)H(\phi)\,dx. \tag{6}$$

In (6), the function ϕ is a continuous signed distance function (SDF) and $H(\phi)$ is the Heavide function of ϕ. In contrast to (5), the minimization problem (6) uses the zero level set of the continuous SDF to represent a contour. Such curve representation allows to calculate the geometric features of a curve such as normal and curvature more naturally than the relaxed binary representation used in (5). However, (6) may be more complicated than (5) when discretised for a numerical solution.

In the following, we combine both (5) and (6) and propose to solve the following minimization problem for image segmentation:

$$\min_{u,\phi} \int_\Omega g(\phi)\,|\nabla u|\,dx + \int_\Omega Q(c_1,c_2)u dx, \tag{7}$$

under constraints:

$$u = H(\phi),$$

with

$$g(\phi) = \alpha + \beta \left| \nabla \cdot \frac{\nabla \phi}{|\nabla \phi|} \right|^2. \tag{8}$$

In the above, we still need the function ϕ to be a signed distance function. Note that we use the binary function u to express the length term and the SDF function ϕ to calculate the curvature values. The minimization problem (7) has two unknowns and we shall use an alternating minimization like procedure to solve it. First we fix ϕ^k and optimize the following functional to get u^{k+1}

$$u^{k+1} = \underset{u \in \{0,1\}}{\operatorname{argmin}} \int_\Omega g\left(\phi^k\right) |\nabla u| \, dx + \int_\Omega Q\left(c_1, c_2\right) u dx. \tag{9}$$

Then u^{k+1} is fixed and we solve ϕ^{k+1} from

$$u^{k+1} = H(\phi^{k+1}).$$

Given the binary function u^{k+1}, there is a unique SDF ϕ^{k+1} satisfying the above relation and we denote this relationship by:

$$\phi^{k+1} = SDF\left(u^{k+1}\right). \tag{10}$$

Note that problem (9) is non-convex due to the binary constraint. It is known from [25] that it is equivalent to the following convex problem:

$$u^{k+1} = \underset{u \in [0,1]}{\operatorname{argmin}} \int_\Omega g\left(\phi^k\right) |\nabla u| \, dx + \int_\Omega Q\left(c_1, c_2\right) u dx \tag{11}$$

in the sense that a threshold of a solution of (11) by a value $\mu \in (0,1)$ gives a global minimizer for (9). Let us take $\mu = 0.5$ as the threshold value in this paper. Then ϕ^{k+1} in (10) can be easily calculated by a re-distance process which can be efficiently solved by the fast marching method [26, 27] or the fast sweeping method [28, 29, 30]. The latter is adopted in this paper.

Unfortunately, as the contour evolution speed using the binary function u is too fast and the numerical computation can be unstable for the proposed model (7). To circumvent this drawback, we add another term to (9) and then we have to solve:

$$u^{k+1} = \underset{u \in [0,1]}{\operatorname{argmin}} \int_\Omega g\left(\phi^k\right) |\nabla u| \, dx + \int_\Omega Q\left(c_1, c_2\right) u dx + \frac{\theta}{2} \int_\Omega \left(u - u^k\right)^2 dx. \tag{12}$$

The positive parameter θ controls the similarity between u^{k+1} and u^k. Larger θ results in smaller changes between u^{k+1} and u^k and thus contour evolutes slowly and steadily.

Note that (12) is a total variation minimization problem with a simple fidelity term which is essentially similar to the ROF model. Nowadays, there are many fast algorithms available to solve this problem. It is clear to see that our algorithm is very easy to implement and it just needs a ROF model solver and a re-distance solver. In addition, we have very few parameters to tune compared to other fast numerical algorithms for minimizing the elastica energy.

The minimizer for the proposed model (7) shall be found by iterating (12) and (10) until the system converges. For clarity, we present the overall algorithm for the Euler's elastica energy segmentation as follows.

Algorithm 1 Euler's Elastica energy for Image Segmentation

1: **Input:** f, u^0, a, b, θ
2: **while** *some stopping criteria is not satisfied* **do** ▷ Criteria can be relative error of ϕ
3: Update u^{k+1} via (12) ▷ Use fast total variation solvers
4: Update ϕ^{k+1} via Eq. (10) ▷ Use fast sweep method
5: Update $g(\phi^{k+1})$ via Eq. (8)
6: **end while**
7: **return** optimal u^{k+1} ▷ Extract the interface from u^{k+1}

2.2. Image Inpainting. In this section, we shall try to use similar ideas as were used in the last section for image inpainting, especially for inpaninting and smoothing of binary images. More precisely, let f be a given binary image defined on an image domain Ω with image information in the region B missing. The problem is to mathematically reconstruct the original image u in the damaged domain $B \subset \Omega$, using the following model involving Euler's elastica energy:

$$\min_{u\in\{0,1\},\phi} \int_\Omega g(\phi)\,|\nabla u|\,dx + \int_\Omega \lambda_B (u-f)^2 dx, \tag{13}$$

under constraints:

$$u = H(\phi),$$

with $g(\phi)$ being as defined in (8) and λ_B be given in the form:

$$\lambda_B(x) = \begin{cases} 1 & x \in \Omega\backslash B \\ 0 & x \in B \end{cases}.$$

In (13), the fidelity term $\mathcal{D}(u) = \int_\Omega \lambda_B (u-f)^2 dx$ is used, which forces the minimizer u to stay close to the given binary image f outside of the inpainting domain $\Omega\backslash B$ (how close depends on the values of a and b in the regulariser). While inside the broken region B, the regulariser plays the main role of filling in the missing content. Using such Euler's elastica regulariser, the inapinting model is capable of interpolating large gaps of objects and making smooth connection along the level curves of images in inpainting domains, so the inpainting results can be satisfactory for the human visual system. Note that the variational approach (13) acts on the whole image domain, instead of posing the problem only on the broke region B. This makes the approach independent of the number and shape of the holes/gaps in the image. Even more, it eliminates the difficulties related to boundary conditions on the inpainting region B.

The problem (13) with its constraints can be optimized in a manner analogous to (7). First, ϕ is fixed to minimize u^{k+1}, which is given as

$$u^{k+1} = \operatorname*{argmin}_{u\in\{0,1\}} \int_\Omega g\left(\phi^k\right)|\nabla u|\,dx + \int_\Omega \lambda_B (u-f)^2 dx. \tag{14}$$

To guarantee the stability of numerical computation, an additional term is added to the inpainting model (14)

$$u^{k+1} = \operatorname*{argmin}_{u\in[0,1]} \int_\Omega g\left(\phi^k\right)|\nabla u|\,dx + \int_\Omega \lambda_B (u-f)^2 dx + \frac{\theta}{2}\int_\Omega (u-u^k)^2 dx. \tag{15}$$

Note that in (15) we have also relaxed the binary constraint. In addition, (15) is a ROF inpainting model which can be efficiently minimized by the well-established

solvers. After u^{k+1} is obtained, $\phi's$ update follows the following equation

$$\phi^{k+1} = SDF\left(u^{k+1}\right), \tag{16}$$

which can be iteratively solved by using the fast sweep method to the 0.5 level set of u^{k+1} calculated from (15). After ϕ^{k+1} is updated from (16), we go back to update u^{k+1} from (15) again. This procedure is repeated until the convergence is achieved. Lastly, we present the overall algorithm for the Euler's elastica inpainting energy as follows.

Algorithm 2 Euler's Elastica for Image Inpainting

1: **Input:** f, λ_B, u^0, a, b, θ
2: **while** *some stopping criteria is not satisfied* **do** ▷ Criteria can be relative error of ϕ
3: Update u^{k+1} via (15) ▷ Use fast total variation solvers
4: Update ϕ^{k+1} via Eq. (16) ▷ Use fast sweep method
5: Update $g(\phi^{k+1})$ via Eq. (8)
6: **end while**
7: **return** optimal u^{k+1} ▷ Extract the interface from u^{k+1}

2.3. Illusory Shapes via Corner Fusion. Illusory shapes (or contours) are visual illusions that evoke the perception of a shape without a luminance or color change over that shape. A famous illusory example (Kanizsa triangle) has been shown in the left image of Figure 1, where our visual system allows us to see an illusory triangle, as shown in the middle (coloured in gray for visibility). The perceptibility of illusory shapes reveals the powerful capability of the human vision system. As vision system is connected to brain, studies on illusory shapes often play an important role in contemporary brain and cognitive sciences.

FIGURE 1. Kanizsa's Triangle (left). These spatially separate shapes give the impression of a white triangle, defined by a sharp illusory contour. The middle image shows such illusory triangle which occludes the three black circles in the right.

Many researchers have developed quantitative models and algorithms for automatic or semi-automatic detection of illusory shapes. Among them variational PDE approaches [31, 32, 33, 8] are commonly employed. These methods are either image- or edge-based models, which normally involve computational tools such as active contours [32], curvatures, domain acttraction, and level set implementation [33, 8]. More specifically, an semi-automatic variational method was proposed by the authors in [34], where they first define corner bases using manually selected corner points and then reconstruct illusory shapes from images using the elastica phase field theory. In contrast to the phase field, we intent to extract illusory

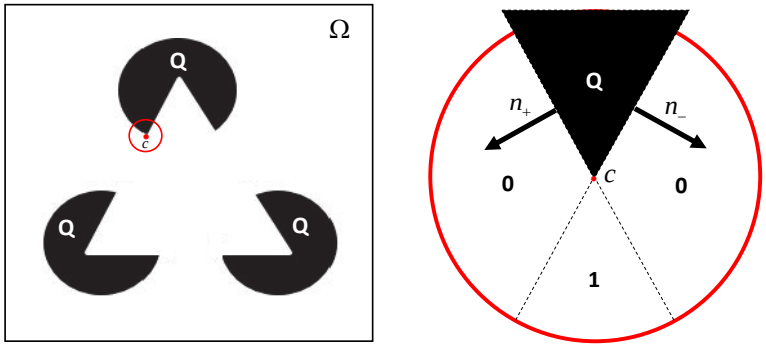

FIGURE 2. Illustration on how to construct a convex corer using pre- and post-normal vectors. The right image is a zoom-in version of the red circle in the left. The red dot in the images represents the corner c.

shapes by using the Euler's elastica regulariser introduced above, together with the the fidelity term defined by the corner base technique [34].

Here, we explain some details on how to define the corner bases as given in [34]. First, we use Q to denote the region for the given shapes, see the black regions in Figure 2. Let c be a given corner of Q ($c \in \angle Q$) with pre- and post-normal vectors $\boldsymbol{n}_-$ and $\boldsymbol{n}_+$, respectively. For any $r > 0$, the r-corner base $\mathcal{B}(c)$ at c is defined: First the base $\mathcal{B}(c) = (R(c), f_c)$ is the r-disk under the given norm $R(c) = x : \|x - c\| \leq r$; Second the corner signature f_c is defined on $\mathcal{B}(c)$ via

$$f_c(x) = \begin{cases} 1 & \boldsymbol{n}_- \cdot (x - c) \geq 0 \text{ and } \boldsymbol{n}_+ \cdot (x - c) \geq 0 \\ 0 & \text{otherwise} \end{cases}. \tag{17}$$

Based on the concept of the corner base defined above, we propose to minimize the following objective energy minimization model for illusory shape reconstruction.

$$\min_{u \in \{0,1\}, \phi} \int_{\Omega \backslash Q} g(\phi) |\nabla u| \, dx + \sum_{c \in \angle Q} \int_{R(c) \backslash Q} (u - f_c)^2 dx. \tag{18}$$

Note that in (18) the new fidelity term $\mathcal{D}(u)$ involves using multiple corners of Q. The regulariser and fidelity term in (18) are defined over different computational domains and it is therefore difficult to optimise it. By making using of the indicator function λ_c, these two energy terms can act on the same image domain $\Omega \backslash Q$ (see Figure 2 left). An equivalent form of (18) is thus given by

$$\min_{u \in \{0,1\}, \phi} \int_{\Omega \backslash Q} g(\phi) |\nabla u| \, dx + \sum_{c \in \angle Q} \int_{\Omega \backslash Q} \lambda_c (u - f_c)^2 dx, \tag{19}$$

where $\lambda_c = f_c$. To guarantee the stability of numerical implementation of (19), an additional term is added to (19) in a manner analogous to (12) and (15).

$$\min_{u \in [0,1], \phi} \int_{\Omega \backslash Q} g(\phi) |\nabla u| \, dx + \sum_{c \in \angle Q} \int_{\Omega \backslash Q} \lambda_c (u - f_c)^2 dx + \frac{\theta}{2} \int_{\Omega \backslash Q} (u - u^k)^2 dx. \tag{20}$$

Note that in (20) the binary constraint has been relaxed to the interval $[0, 1]$ to guarantee a global solution to (20). By introducing another indicator function

to (20), the minimization of this problem can be easily transformed into a problem on the whole image domain Ω instead of $\Omega \backslash Q$ and it can be solved by Split-Bregman/Augmeted Lagrangian methods. After u^{k+1} is obtained, $\phi' s$ update follows the following equation

$$\phi^{k+1} = SDF\left(u^{k+1}\right), \tag{21}$$

which can be iteratively solved by using the fast sweep method to the 0.5 level set of u^{k+1} calculated from minimizing (20). The updates of ϕ^{k+1} and u^{k+1} are repeated until the convergence is achieved. Afterwards, the embedded illusory shape can be reconstructed by assembling the inpainted regions accordingly (see Figure 7 for details). Lastly, we present the following overall algorithm for illusory shape restoration via corner fusion.

Algorithm 3 Euler's Elastica for Illusory Shape Reconstruction

1: **Input: Corners** c**,** u^0**,** a**,** b**,** θ
2: Construct corner base f_c and indicator function λ_c via (17).
3: **while** *some stopping criteria is not satisfied* **do** ▷ Criteria can be relative error of ϕ
4: Update u^{k+1} via (20) ▷ Use fast total variation solvers
5: Update ϕ^{k+1} via Eq. (21) ▷ Use fast sweep method
6: Update $g(\phi^{k+1})$ via Eq. (8)
7: **end while**
8: **return** optimal u^{k+1} ▷ Extract the interface from u^{k+1}

3. Experimental Results

FIGURE 3. Segmentation results using **Algorithm 1**. The 2nd and 4th images are the segmented contours of the 1st and 3rd images, respectively.

In this section, numerous experiments are conducted to show the effectiveness of the proposed algorithm for image segmentation (Figure 3-5), image inpainting (Figure 6) and illusory shape reconstruction (Figure 7). We note that the split Bregman method [35, 36, 37, 38], which has been proven to be equivalent to the ALM in [13], is adpoted to minimize (12), (15) and (20) in this work. There are only four parameters in the algorithm, that is, a, b, c and another penalty parameter resulted from the variable split technique. The algorithm therefore requires less efforts from users in terms of parameter tuning.

Figure 3 shows the final segmentation results using the proposed Euler's elastica algorithm. As evident, parts of the circle and the letters "UCLA" are erased. Even though one can easily recognise the shape and the letters, existing segmentation models, such as Chan-Vese's model, might just capture the existing boundaries instead of restoring the missing ones. In image inpainting problems, as shown in Figure 6, missing information of images can be also recovered but the broken

regions must be specified first. In contrast, our segmentation model is capable to interpolate the missing boundaries automatically without specifying the regions.

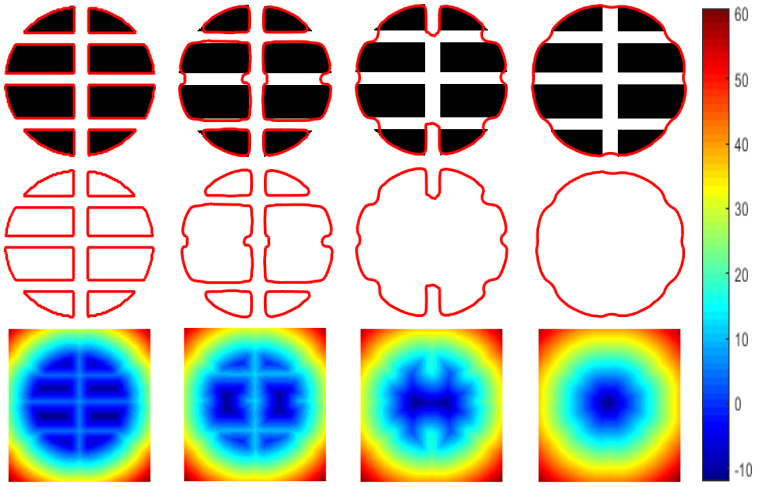

FIGURE 4. Intermediate segmentation results. 1st row: evolving contours overlapping on an incomplete circle. 2nd row: evolving contours alone (0.5 level set of u in (12) at different iteration). 3rd row: SDFs calculated from the corresponding contours in the 2nd row. The color bar at the most right shows the value range of the SDFs in the last row

FIGURE 5. Same as Figure 4, but with the incomplete letters "ULCA".

Figure 4 and 5 show the intermediate contour evolution results and the corresponding signed distance maps. We start the iteration for **Algorithm 1** by using the boundaries of the incomplete object (i.e. circle or UCLA) as the initialisation for u^0. As iteration proceeds, one can observe that the evolving contour is gradually merged together and finally forms an intact shape regardless of the existing gaps within the object. The distance function ϕ in (10), as shown in the last row of Figure 4 and 5, remains a smooth SDF during all the iterations. Such SDF preservation is crucial for the success of the algorithm, because the use of the SDF allows the accurate computation of the curvature of a curve.

Figure 6 shows the inpainting results for some synthetic images and a Chinese handwriting. We note that **Algorithm 2** is now only applicable to binary images.

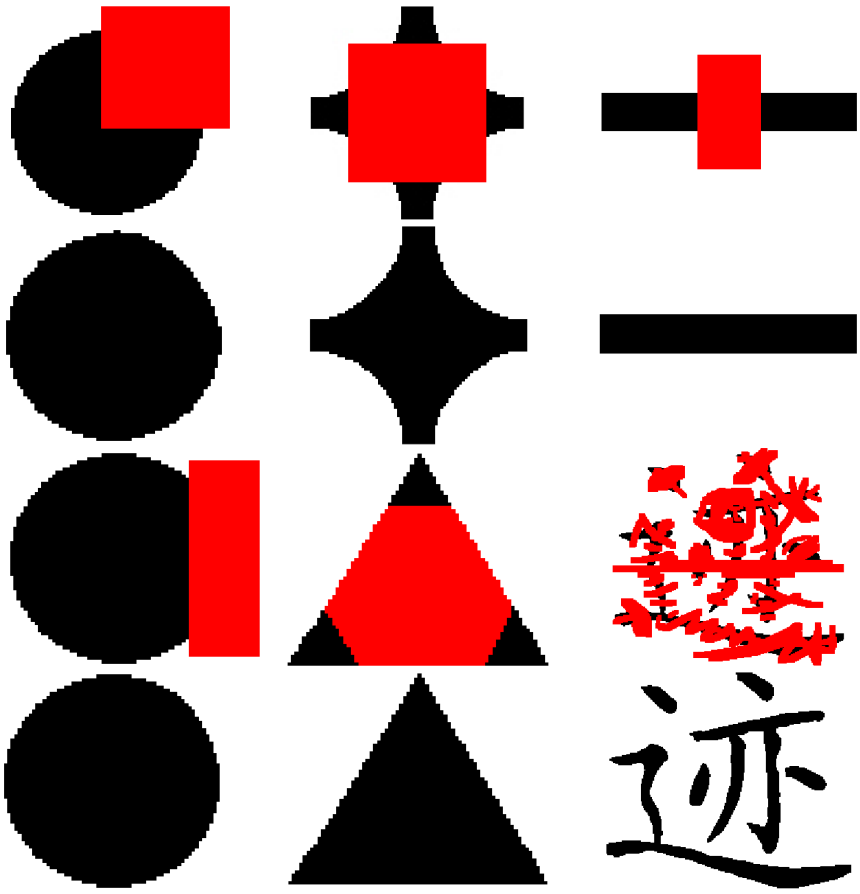

FIGURE 6. Inpainting results using **Algorithm 2**. The 1st and 3rd rows show the damaged images, while the 2nd and 4th rows show the restored images.

The red regions in the first and third rows are the inpainting domains, while the second and fourth rows are inpainting results. As we expect, the Euler's elastica algorithm shows a property of long connectivity and the curvature term makes smooth connection along the level curves of images on inpainting domains. For the Chinese handwritting, we intentionally use complicated shapes for the inpainting domains. Even though in this complex case, the algorithm performs very well. The algorithm is therefore very promising for inpainting the Chinese or Western damaged calligraphy.

Figure 7 shows an illusory triangle reconstruction example using **Algorithm 3**. Based on the corner base technique defined in (17) and the elastica fusion model in (20), we show the output of the model for the Kanizsas Triangle in Figure 1. (a) shows the six corner bases for the Kanizsas Triangle, and (b) shows the optimal elastica field $u > 0.5$ by applying (20) to fuse the six corner bases. Note that in (b) the region plotted in black denotes the optimal elastica field $u < 0.5$, where the connected components are labelled as R_0, R_1, R_2 and R_4. and the gray P region represents $u > 0.5$. With such partitions, the meaningful illusory triangle (e) as well as occluded background objects (f) can be reconstructed.

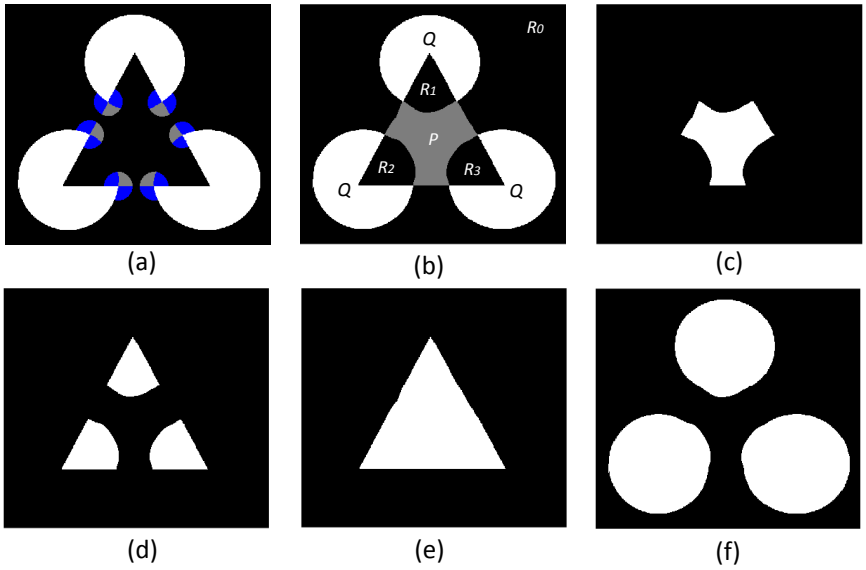

FIGURE 7. Illusory triangle reconstruction using **Algorithm 3**. (a): Kanizsa's triangle overlapped with the corner bases. The pixel values in blue and gray regions are 0 and 1, respectively. (b): Elastica fusion with $u > 0.5$ in gray. (c): P region in (b). (d): R_1, R_2 and R_3 regions in (b). (e): R_1, R_2 and R_3 and P regions in (b). (f): R_1, R_2 and R_3 and Q regions in (b).

4. Conclusion

This work described a very simple algorithm for the minimization of the Euler's elastica energy related variational models. It is well-known that it is difficult to minimize these energies because they involve non-convex, nonlinear, non-differentiate and higher order terms. The new algorithm only needs to solve a total variation type minimization problem and a re-distance problem, which results in fewer built-in parameters. The experimental results indicate that the method yields very good results for image segmentation, image inpainting and illsuroy shape restoration. Due to the simplicity and effectiveness of the proposed algorithm, we believe that it will have promising applications in a number of real industrial problems related to image processing and computer vision.

References

[1] Mark Nitzberg, David Mumford, and Takahiro Shiota. *Filtering, segmentation and depth.*
[2] Jianhong Shen, Sung Ha Kang, and Tony F Chan. Euler's elastica and curvature-based inpainting. *SIAM Journal on Applied Mathematics*, 63(2):564–592, 2003.
[3] Simon Masnou. Disocclusion: a variational approach using level lines. *IEEE Transactions on Image Processing*, 11(2):68–76, 2002.
[4] Xue-Cheng Tai, Jooyoung Hahn, and Ginmo Jason Chung. A fast algorithm for euler's elastica model using augmented lagrangian method. *SIAM Journal on Imaging Sciences*, 4(1):313–344, 2011.
[5] Luigi Ambrosio and Simon Masnou. A direct variational approach to a problem arising in image reconstruction. *Interfaces and Free Boundaries*, 5(1):63–81, 2003.
[6] Luigi Ambrosio and Simon Masnou. On a variational problem arising in image reconstruction. *Free Boundary Problems*, pages 17–26, 2004.
[7] Egil Bae, Juan Shi, and Xue-Cheng Tai. Graph cuts for curvature based image denoising. *IEEE Transactions on Image processing*, 20(5):1199–1210, 2011.

[8] Wei Zhu and Tony Chan. A variational model for capturing illusory contours using curvature. *Journal of Mathematical Imaging and Vision*, 27(1):29–40, 2007.

[9] Wei Zhu, Xue-Cheng Tai, and Tony Chan. Image segmentation using eulers elastica as the regularization. *Journal of scientific computing*, 57(2):414–438, 2013.

[10] Egil Bae, Xue-Cheng Tai, and Wei Zhu. Augmented lagrangian method for an eulers elastica based segmentation model that promotes convex contours. *Inverse Problems and Imaging*, 11(1):1–23, 2017.

[11] Carlos Brito-Loeza and Ke Chen. Multigrid algorithm for high order denoising. *SIAM Journal on Imaging Sciences*, 3(3):363–389, 2010.

[12] Fenlin Yang, Ke Chen, and Bo Yu. Homotopy method for a mean curvature-based denoising model. *Applied Numerical Mathematics*, 62(3):185–200, 2012.

[13] Chunlin Wu and Xue-Cheng Tai. Augmented lagrangian method, dual methods, and split bregman iteration for rof, vectorial tv, and high order models. *SIAM Journal on Imaging Sciences*, 3(3):300–339, 2010.

[14] Wei Zhu, Xue-Cheng Tai, and Tony Chan. Augmented lagrangian method for a mean curvature based image denoising model. *Inverse problems and imaging*, 7(4):1409–1432, 2013.

[15] Noha Youssry El-Zehiry and Leo Grady. Fast global optimization of curvature. In *Computer Vision and Pattern Recognition (CVPR), 2010 IEEE Conference on*, pages 3257–3264. IEEE, 2010.

[16] Kristian Bredies, Thomas Pock, and Benedikt Wirth. A convex, lower semicontinuous approximation of euler's elastica energy. *SIAM Journal on Mathematical Analysis*, 47(1):566–613, 2015.

[17] Evgeny Strekalovskiy and Daniel Cremers. Generalized ordering constraints for multilabel optimization. In *Computer Vision (ICCV), 2011 IEEE International Conference on*, pages 2619–2626. IEEE, 2011.

[18] Thomas Schoenemann, Fredrik Kahl, and Daniel Cremers. Curvature regularity for region-based image segmentation and inpainting: A linear programming relaxation. In *Computer Vision, 2009 IEEE 12th International Conference on*, pages 17–23. IEEE, 2009.

[19] Thomas Schoenemann, Fredrik Kahl, Simon Masnou, and Daniel Cremers. A linear framework for region-based image segmentation and inpainting involving curvature penalization. *International Journal of Computer Vision*, 99(1):53–68, 2012.

[20] Stanley Osher and James A Sethian. Fronts propagating with curvature-dependent speed: algorithms based on hamilton-jacobi formulations. *Journal of computational physics*, 79(1):12–49, 1988.

[21] Wenqi Lu, Jinming Duan, Zhaowen Qiu, Zhenkuan Pan, Ryan Wen Liu, and Li Bai. Implementation of high-order variational models made easy for image processing. *Mathematical Methods in the Applied Sciences*, 2016.

[22] Tony F Chan and Luminita A Vese. Active contours without edges. *IEEE Transactions on image processing*, 10(2):266–277, 2001.

[23] Wei Zhu, Tony Chan, and Selim Esedo g¯ lu. Segmentation with depth: A level set approach. *SIAM journal on scientific computing*, 28(5):1957–1973, 2006.

[24] Lu Tan, Zhenkuan Pan, Wanquan Liu, Jinming Duan, Weibo Wei, and Guodong Wang. Image segmentation with depth information via simplified variational level set formulation. *Journal of Mathematical Imaging and Vision*, pages 1–17, 2017.

[25] Tony F Chan, Selim Esedoglu, and Mila Nikolova. Algorithms for finding global minimizers of image segmentation and denoising models. *SIAM journal on applied mathematics*, 66(5):1632–1648, 2006.

[26] James A Sethian. A fast marching level set method for monotonically advancing fronts. *Proceedings of the National Academy of Sciences*, 93(4):1591–1595, 1996.

[27] James Albert Sethian. *Level set methods and fast marching methods: evolving interfaces in computational geometry, fluid mechanics, computer vision, and materials science*, volume 3. Cambridge university press, 1999.

[28] Yen-Hsi Richard Tsai, Li-Tien Cheng, Stanley Osher, and Hong-Kai Zhao. Fast sweeping algorithms for a class of hamilton–jacobi equations. *SIAM journal on numerical analysis*, 41(2):673–694, 2003.

[29] Hongkai Zhao. A fast sweeping method for eikonal equations. *Mathematics of computation*, 74(250):603–627, 2005.

[30] Jinming Duan, Ben Haines, Wil OC Ward, and Li Bai. Surface reconstruction from point clouds using a novel variational model. In *Research and Development in Intelligent Systems XXXII*, pages 135–146. Springer, 2015.

[31] Yoon Mo Jung and Jianhong Jackie Shen. First-order modeling and stability analysis of illusory contours. *Journal of Visual Communication and Image Representation*, 19(1):42–55, 2008.
[32] Alessandro Sarti, Ravi Malladi, and James A. Sethian. Subjective surfaces: a geometric model for boundary completion. *International Journal of Computer Vision*, 46(3):201–221, 2002.
[33] Wei Zhu and Tony Chan. A Variational Model for Capturing Illusory Contours Using Curvature. *Journal of Mathematical Imaging and Vision*, 27(1):29–40, sep 2006.
[34] Sung Ha Kang, Wei Zhu, and Jackie Jianhong. Illusory shapes via corner fusion. *SIAM Journal on Imaging Sciences*, 7(4):1907–1936, 2014.
[35] Tom Goldstein and Stanley Osher. The split bregman method for l1-regularized problems. *SIAM journal on imaging sciences*, 2(2):323–343, 2009.
[36] Jinming Duan, Zhenkuan Pan, Baochang Zhang, Wanquan Liu, and Xue-Cheng Tai. Fast algorithm for color texture image inpainting using the non-local ctv model. *Journal of Global Optimization*, 62(4):853–876, 2015.
[37] Jinming Duan, Zhaowen Qiu, Wenqi Lu, Guodong Wang, Zhenkuan Pan, and Li Bai. An edge-weighted second order variational model for image decomposition. *Digital Signal Processing*, 49:162–181, 2016.
[38] Jinming Duan, Christopher Tench, Irene Gottlob, Frank Proudlock, and Li Bai. New variational image decomposition model for simultaneously denoising and segmenting optical coherence tomography images. *Physics in medicine and biology*, 60(22):8901, 2015.

Department of Mathematics, Hong Kong Baptist University, Kowloon Tong, Hong Kong
E-mail: xuechengtai@hkbu.edu.hk

School of Computer Science, University of Nottingham, Nottingham, United Kingdom
E-mail: Jinming.Duan@nottingham.ac.uk